

Electronic Supplementary Information (ESI)

High-fidelity detection of Picric acid following proton prompted fluorescence quenching by a novel acridine yellow G based binuclear Zn^{II}-metallacycle

Prem Chand and Ashish Kumar*

Department of Chemistry, Institute of science, Banaras Hindu University, Varanasi – 221005

U. P., India. *E-mail:* akumar.chem@bhu.ac.in.

S. No.	Figures	Page No.
1	Fig. S1	2
2	Fig. S2	3
3	Fig. S3 & S4	4-5
4	Fig. S5 & S6	6-7
5	Fig. S7	8
6	Fig. S8	9
7	Fig. S9 & S10	10
9	Fig. S11	11
10	Fig. S12	12
11	Fig. S13	12
12	Fig. S14	13
13	Fig. S15 & S16	14
14	Fig. S17	14
15	Fig. S18 & S19	15
16	Fig. S20 & S21	16
17	Fig. S22	17
18	Fig. S23	18
19	Fig. S24 & S25	19
20	Fig. S26 & S27	20
21	Table T1-T3	21-23
22	Table T4	24
23	References	25

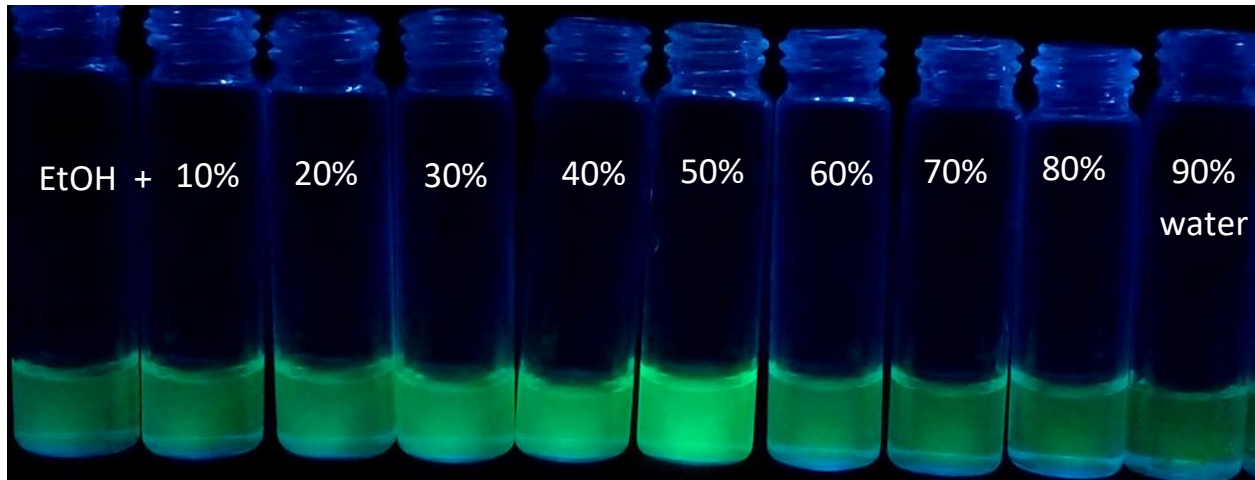


Fig. S1 Display of fluorescence for complex **1** in EtOH/H₂O mixture with increasing % ratio of H₂O in EtOH from 0 to 90% which showed maximum fluorescence in 50% EtOH/H₂O ratio.

Determination of quantum yield:

Quantum yields for **H₂L**, **H₂L_M**, **1** and **2** were determined by using quinine sulphate ($\Phi = 0.54$, 1 M H₂SO₄) as an internal standard in aqueous ethanolic solution (c, 1.0×10^{-5} M: v/v, 1/1) according to the following equation¹⁻²:

$$Q = Q_R \cdot I / I_R \cdot OD_R / OD \cdot \eta^2 / \eta^2_R$$

Where, Q_R = quantum yield of reference

I = fluorescence intensity area of probe

I_R = fluorescence intensity area of reference

OD_R = optical density of reference

OD = optical density of probe

η^2_R and η^2 are refractive indices of used solutions for reference and probe (EtOH:H₂O)

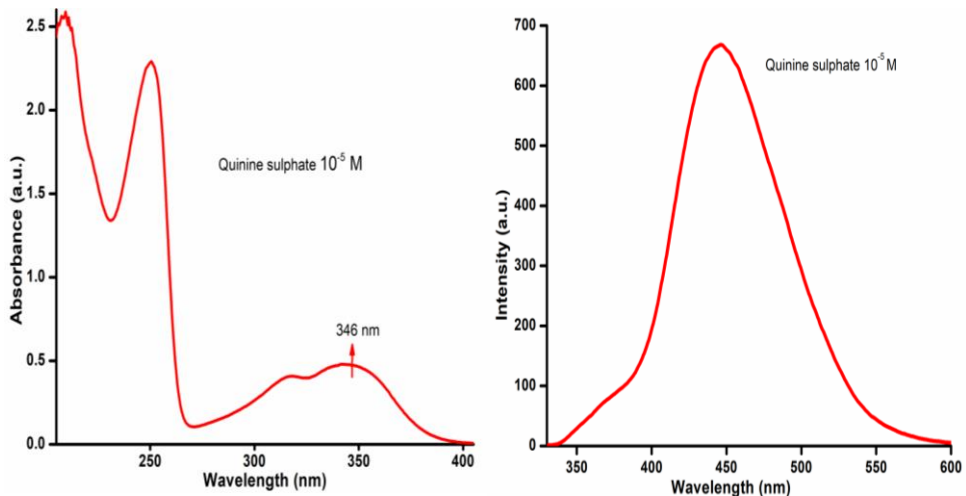


Fig. S2 Absorption and fluorescence spectra for quinine-sulfate recorded in aqueous ethanolic solution of EtOH:H₂O (c, 1.0×10^{-5} M, v/v) which was used as a internal reference for calculation of quantum yield for ligand (H₂L, H₂L_M) and complex (**1**, **2**).

Formulation for percentage fluorescence quenching:

% fluorescence quenching of **1** in presence of all NACs were calculated by using following method.³⁻⁴

$$\text{Quenching} = (I_0 - I)/I_0 \times 100 \%$$

Where, I₀ = Initial fluorescence intensity of **1** in absence of PA

I = Intensity of **1** in presence of PA.

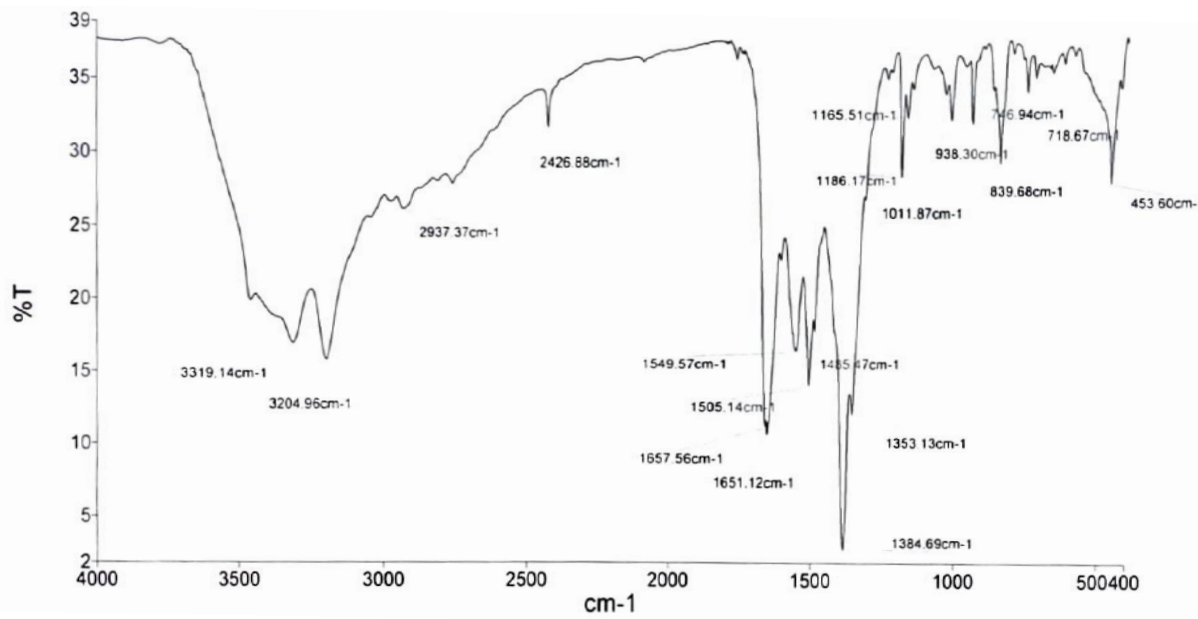
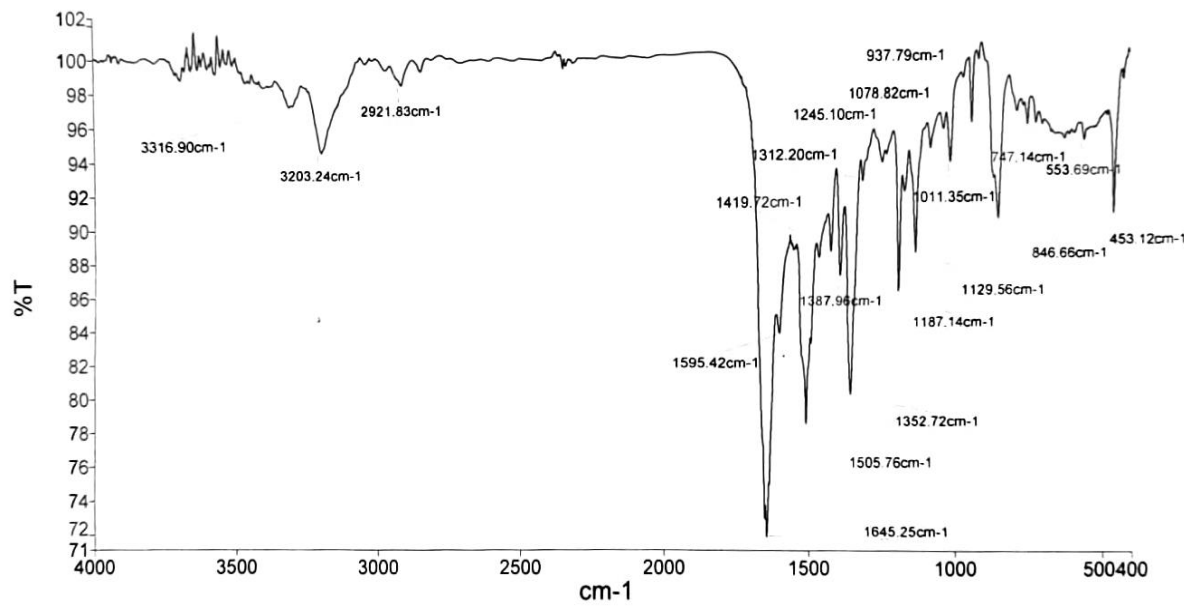


Fig. S3 FT-IR spectra for (a) H_2L and (b) Complex **1**.

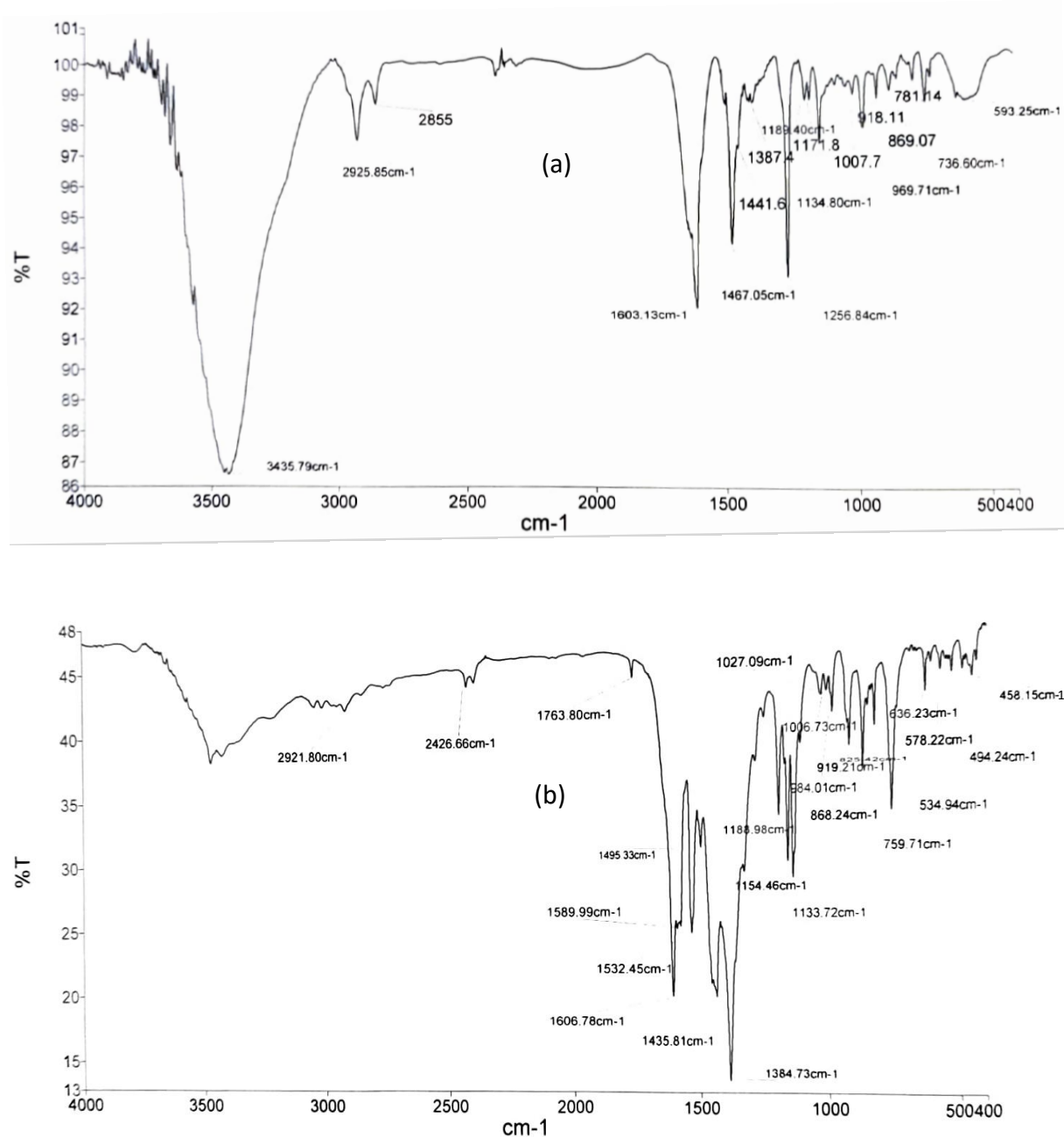


Fig. S4 FT-IR spectra for (a) $\text{H}_2\text{L}_\text{M}$ and (b) Complex 2.

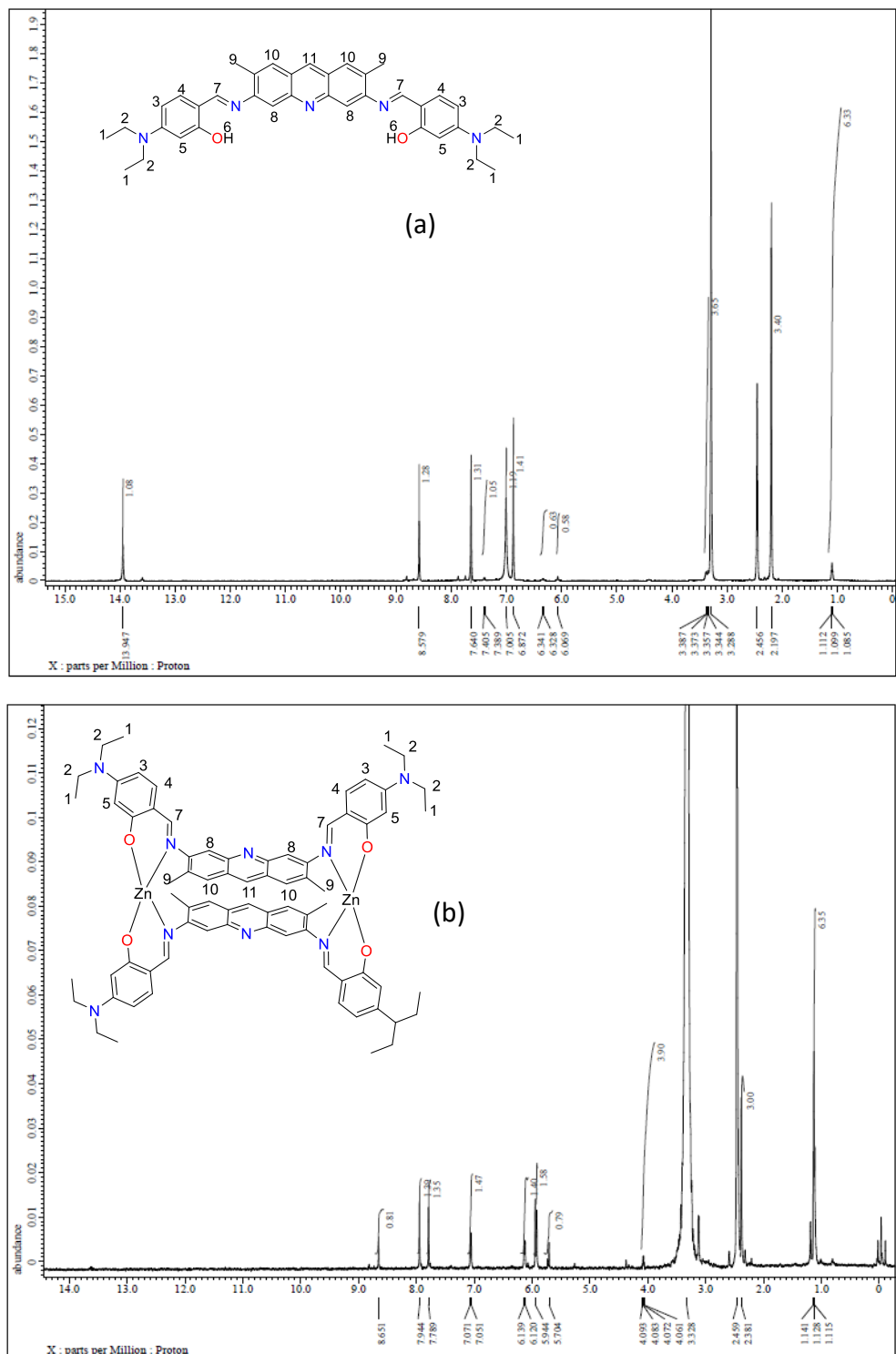


Fig. S5 ^1H -NMR (DMSO-d₆) spectra for (a) **H₂L** and (b) **1** displaying signals for -CH=N- at δ , 8.57 and 8.65 ppm, respectively. The disappearance of signal associated with hydroxyl -OH (δ , 13.94 ppm in **H₂L**) group substantiated the formation of complex **1** from **H₂L**.

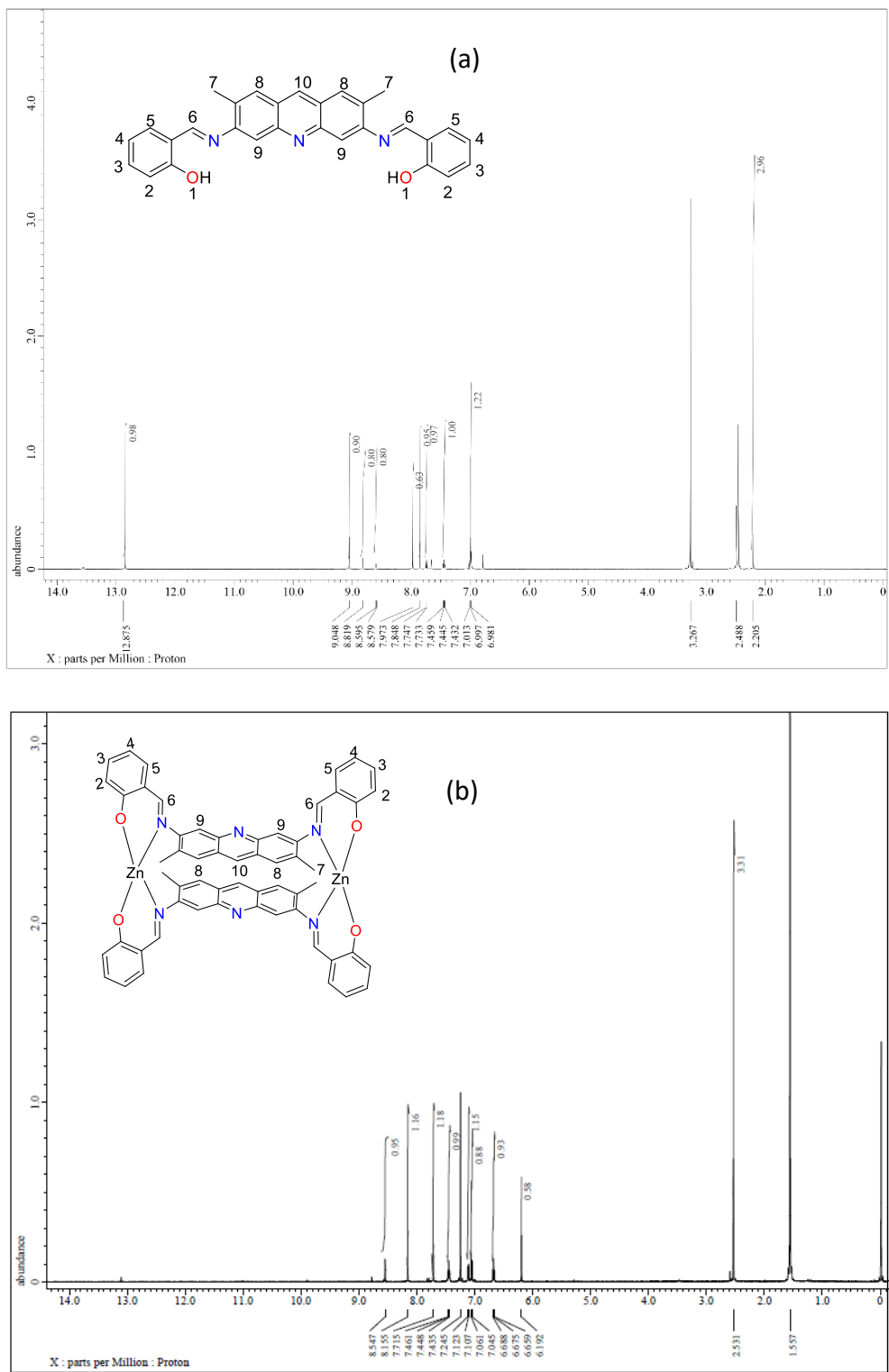


Fig. S6 ¹H-NMR spectra for (a) **H₂L_M** (DMSO-d₆) and (b) Complex **2** (CDCl₃) displaying intact signals for -CH=N- at δ , 9.04 and 8.54 ppm, respectively. The disappearance of signal associated with hydroxyl -OH (δ , 12.87 ppm in **H₂L_M**) group substantiated the formation of complex **2** from **H₂L_M**.

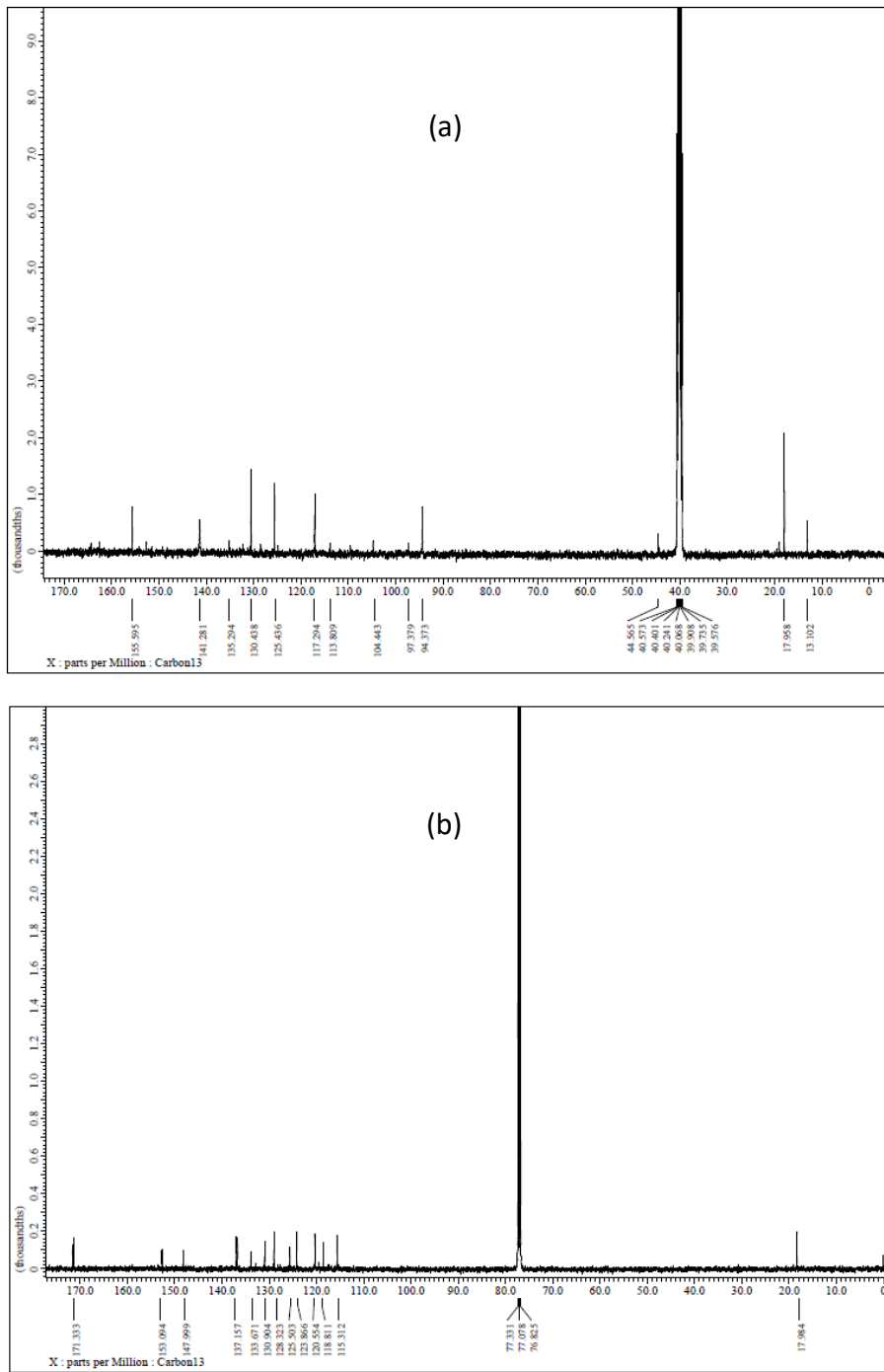


Fig. S7 ¹³C-NMR spectra recorded for (a) **1** $[(\text{ZnL})_2]$ DMSO-d₆ and (b) **2** $[(\text{ZnL}_M)_2]$ in CDCl₃.

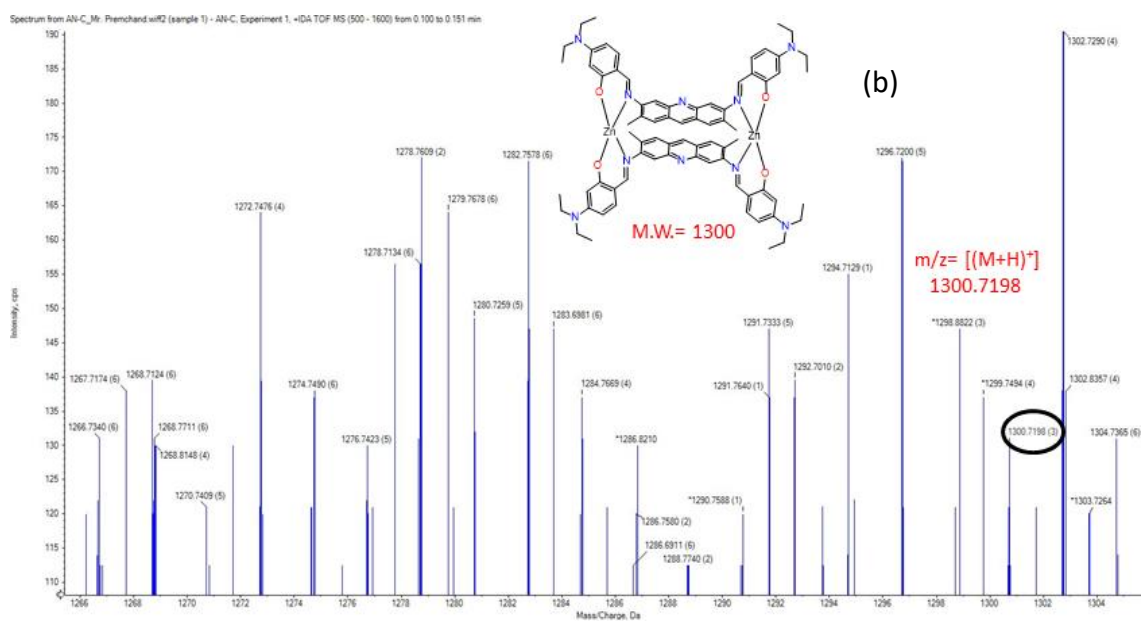
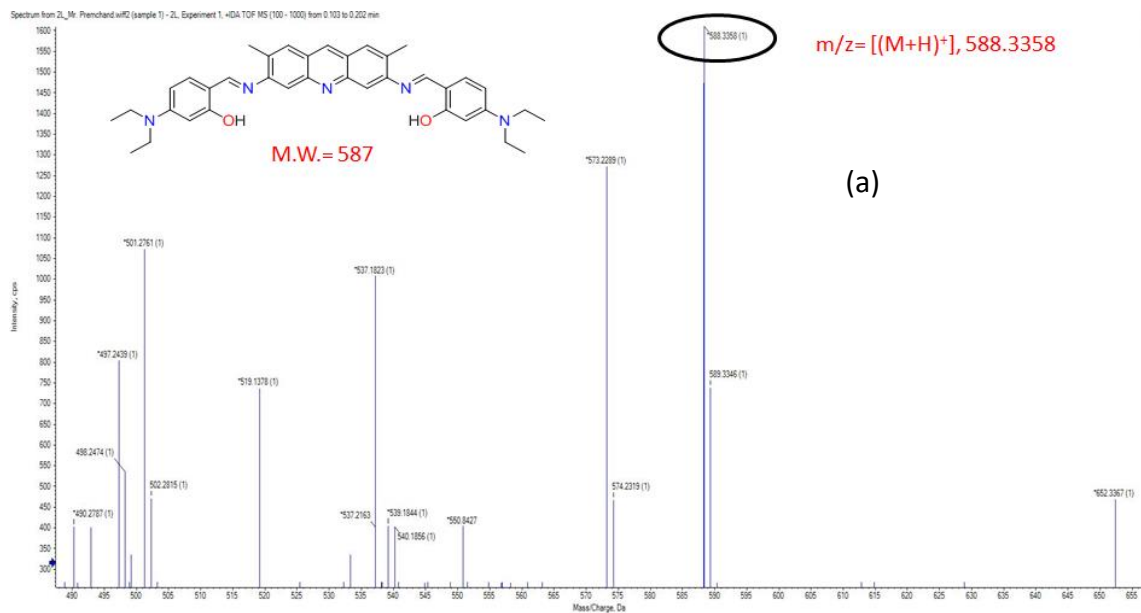


Fig. S8 ESI-Mass (HRMS-QTOF) spectra obtained for (a) H_2L and (b) $\mathbf{1} \cdot [\text{ZnL}]_2$ in positive mode showing molecular ion peaks $[\text{M}+\text{H}]^+$ at m/z 588.3358 and 1300.7198, respectively.

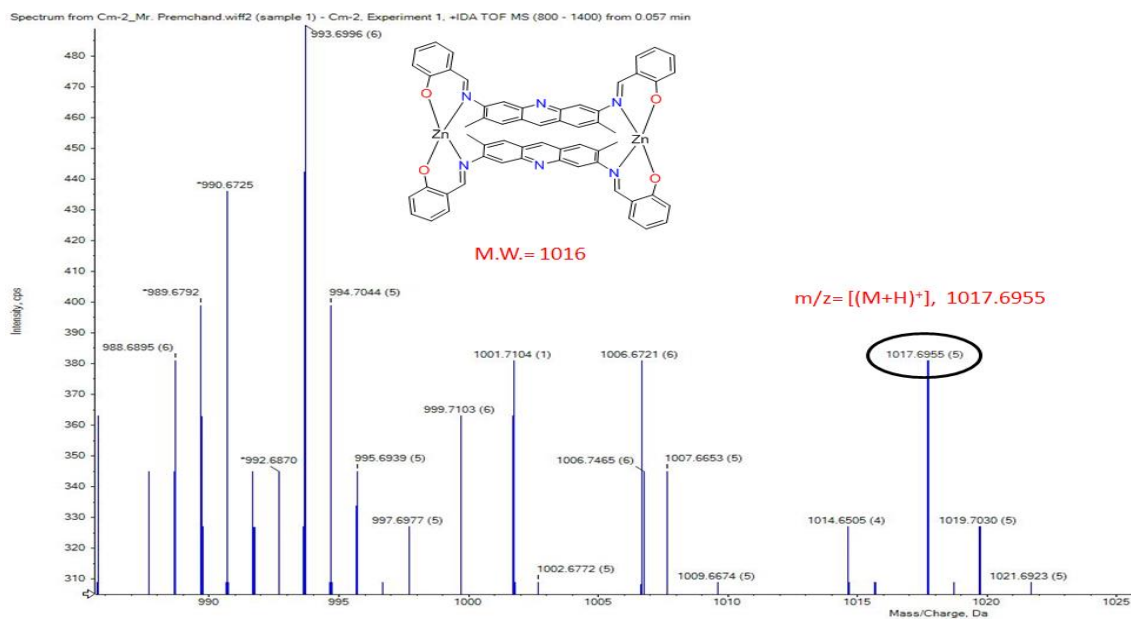


Fig. S9 ESI-Mass (HRMS-QTOF) spectra obtained for **2** $[(\text{ZnL}_M)_2]$ in positive mode showing molecular ion peak $[\text{M}+\text{H}]^+$ at m/z 1017.6955.

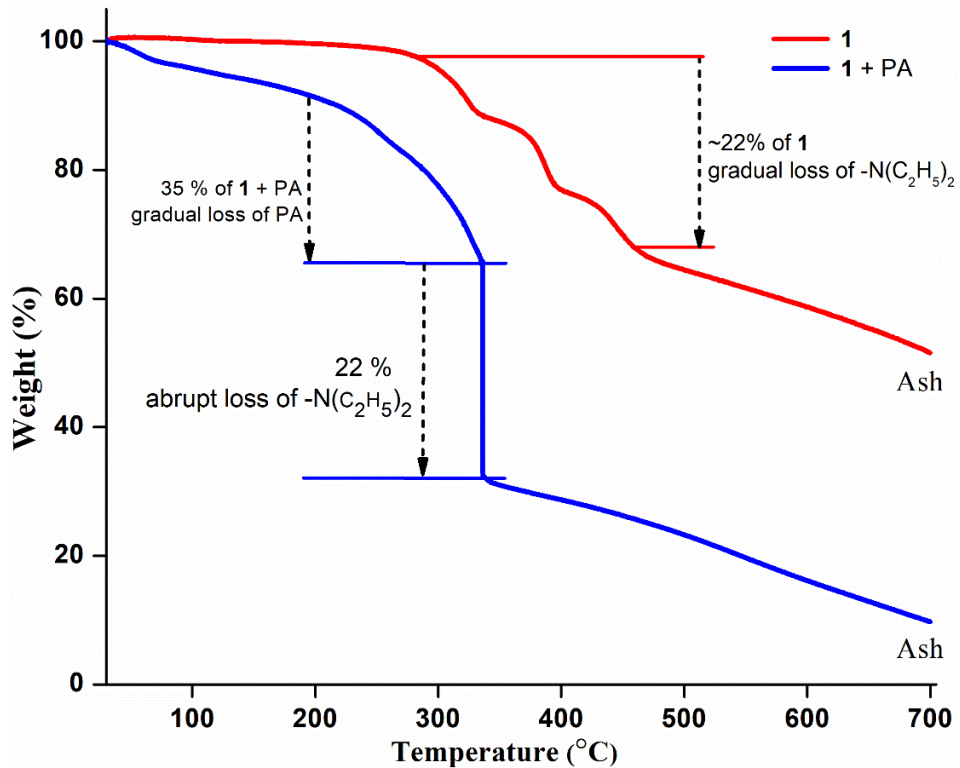


Fig. S10 TGA analysis of **1** and **(1+PA)**. The red curve displays ~22% weight loss signifying gradual decomposition of N,N-diethyl amine from **1** between 283-456 °C. The blue curve showing ~35% and ~22% weight loss indicating most likely the decomposition multiple PA and N,N-diethyl amine moieties between 180-370 °C.

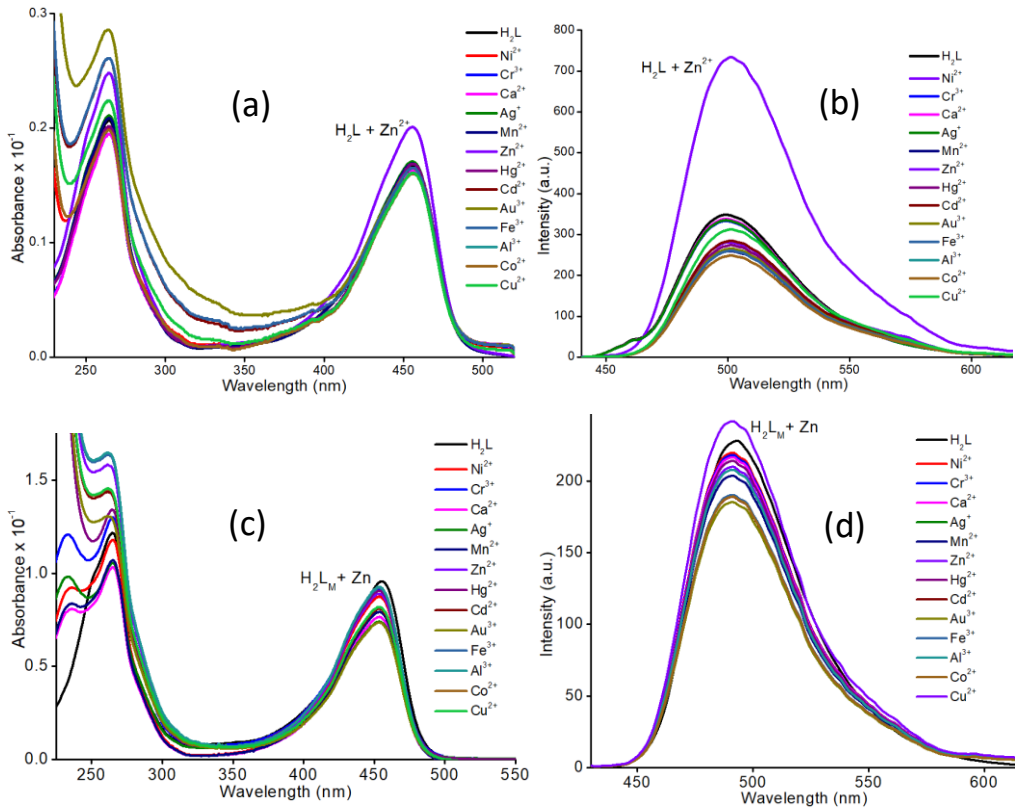


Fig. S11 (a) UV-vis and (b) Fluorescence spectra for H_2L in presence of Ca^{2+} , Cr^{3+} , Mn^{2+} , Fe^{3+} , Co^{2+} , Ni^{2+} , Cu^{2+} , Ag^+ , Au^{3+} , Zn^{2+} , Cd^{2+} , Hg^{2+} and Al^{3+} signifying that significant changes occur only in presence of Zn^{2+} making it most suitable for complex formation. (c) UV-vis and (d) Fluorescence spectra for H_2L_M in presence of Ca^{2+} , Cr^{3+} , Mn^{2+} , Fe^{3+} , Co^{2+} , Ni^{2+} , Cu^{2+} , Ag^+ , Au^{3+} , Zn^{2+} , Cd^{2+} , Hg^{2+} and Al^{3+} . It displayed no significant change with the metal ions. Only a little fluorescence enhancement was observed with Zn^{2+} .

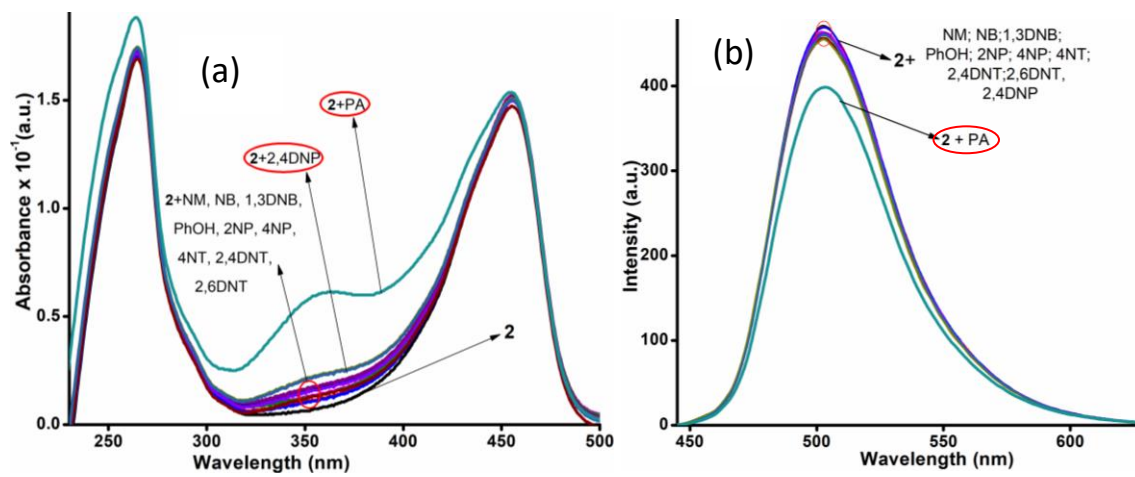


Fig. S12 (a) UV-vis selectivity experiment for **2** in presence of all NACs which showed negligible change in spectral feature of **2** in presence of all NACs including PA. (b) Insignificant changes in fluorescence spectra for **2** in presence of all NACs including PA. Though, PA offered some moderate alteration in spectra, it was insignificant in comparison to **1**.

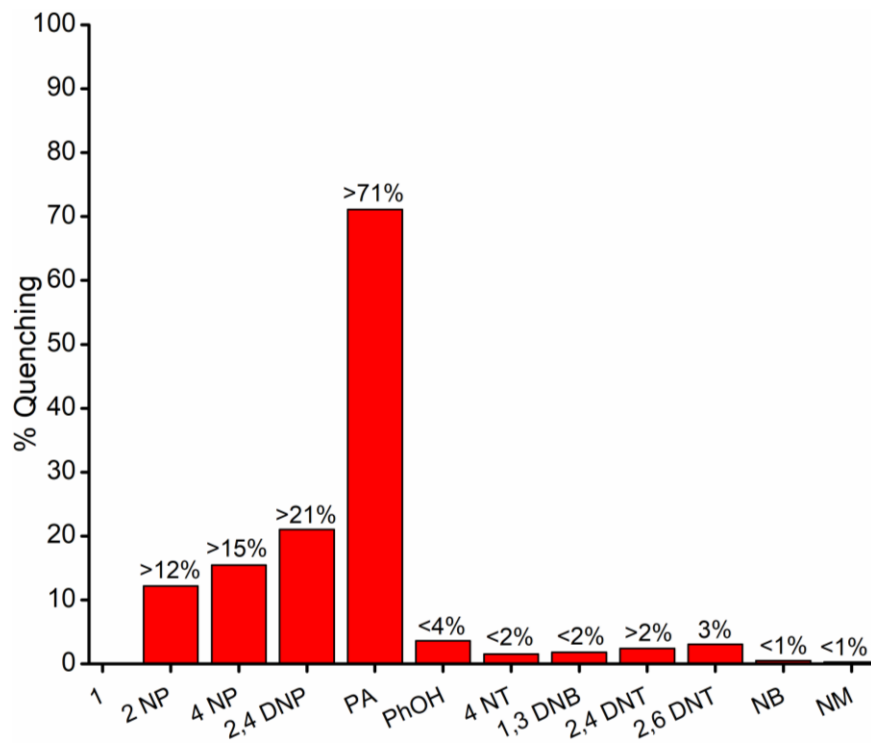


Fig. S13 Bar diagram showing comparative fluorescence quenching capacities of NACs with **1**. PA shown substantial changes (>71%) among all.

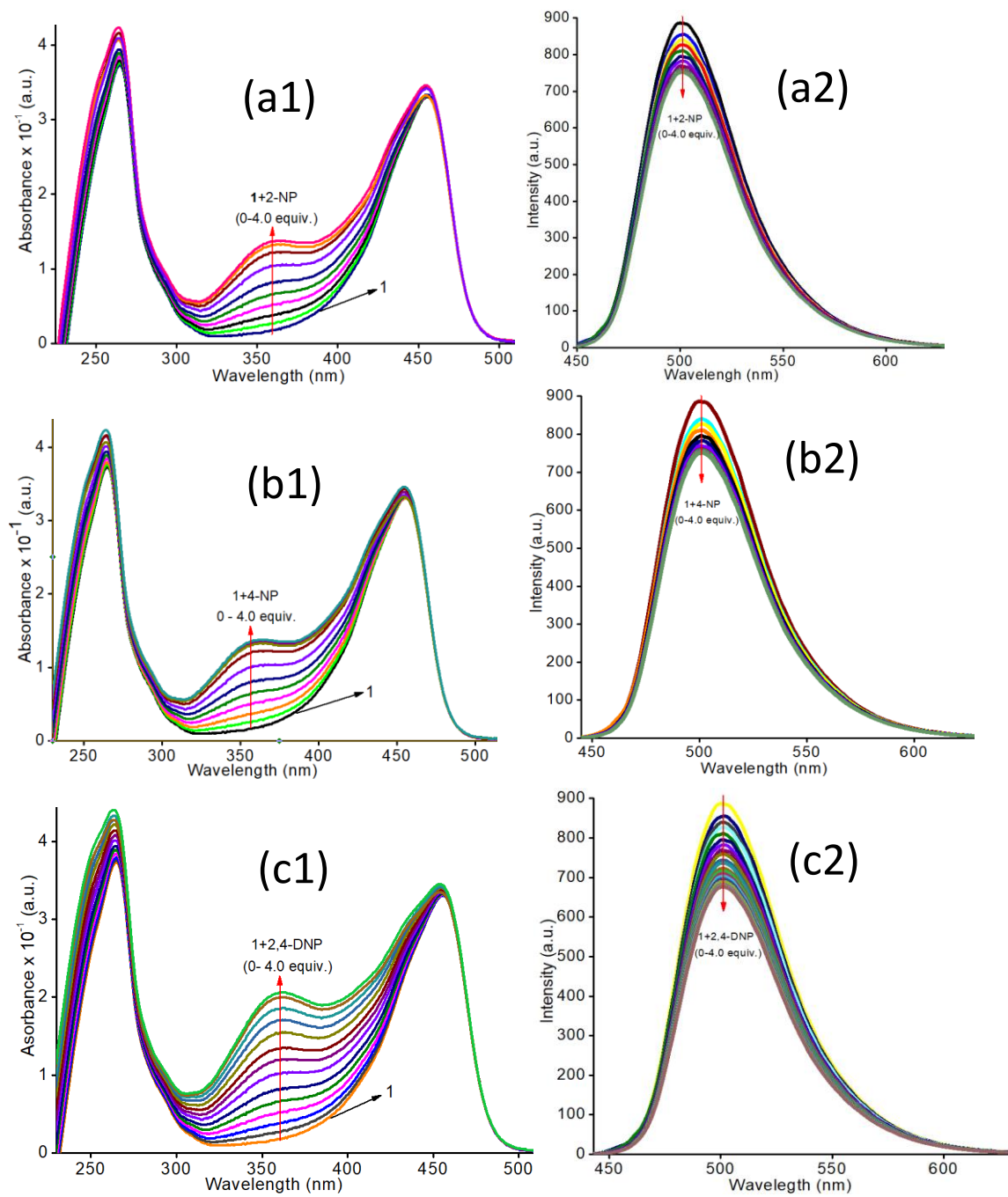


Fig. S14 (a1) UV-vis and (a2) Fluorescence titration spectral for **1+2-NP**. (b1) UV-vis and (a2) Fluorescence titration spectra for **1+4-NP**. (c1) UV-vis and (c2) Fluorescence titration spectra for **1+2,4-DNP**.

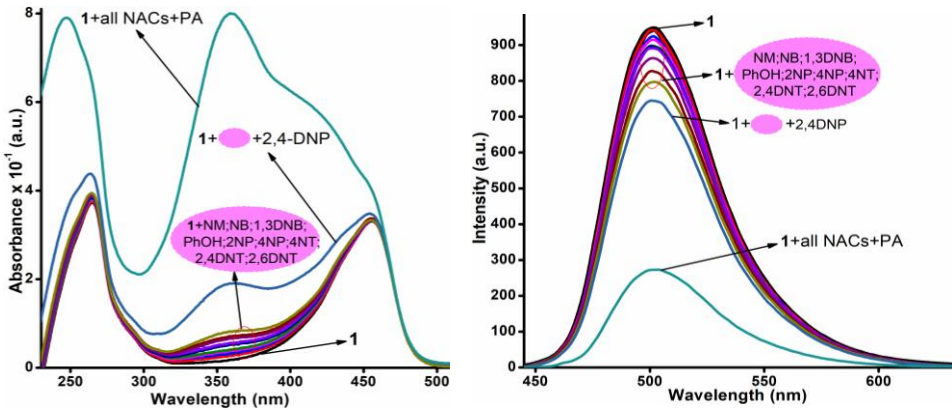


Fig. S15 UV-vis and fluorescence experiments showing negligible interference in collective presence of all NACs for PA (**1** + all NACs + PA).

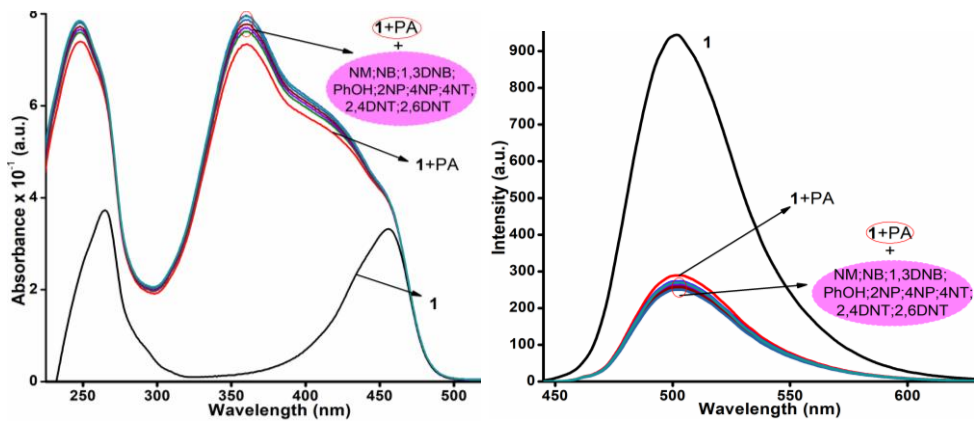


Fig. S16 UV-vis and fluorescence experiments showing negligible change after addition of PA into **1** due to all NACs (**1** + PA + all NACs).

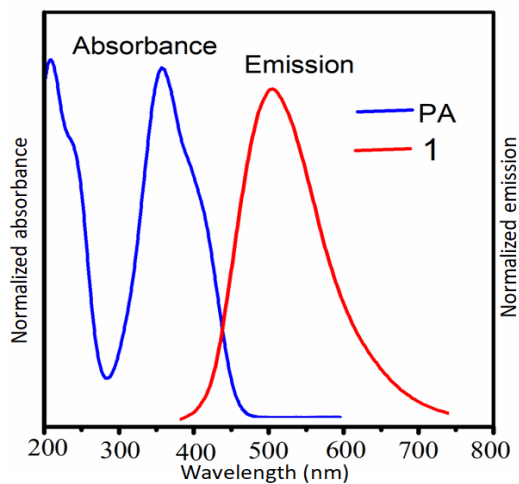


Fig. S17 Normalized UV-vis spectrum for PA and fluorescence spectrum for **1**.

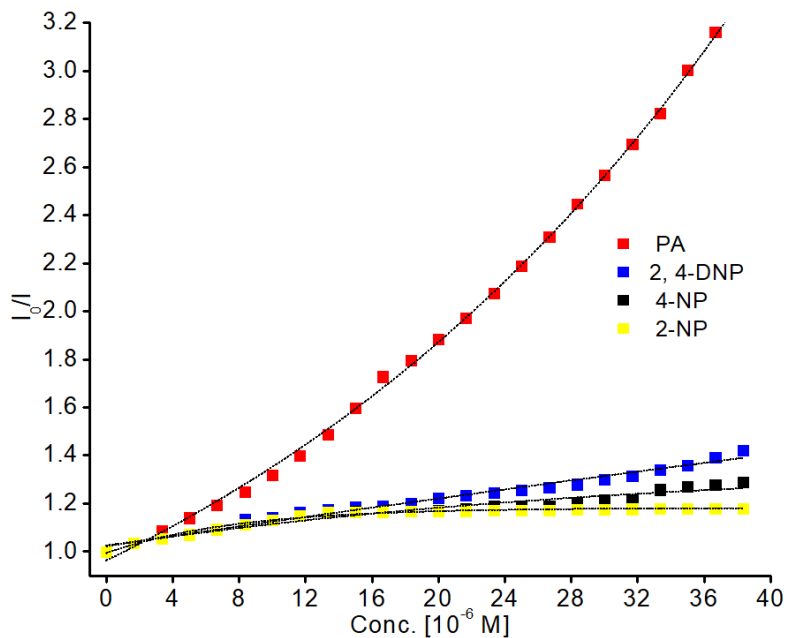


Fig. S18 Non-linear S-V plots for **1** ($c, 1.0 \times 10^{-5}$ M) in EtOH/H₂O in presence of PA; 2,4-DNP; 4-NP; and 2-NP between 0 to 38.33×10^{-5} M concentration showing excellent quenching affinities of PA than 2,4-DNP, 4-NP and 2-NP, respectively .

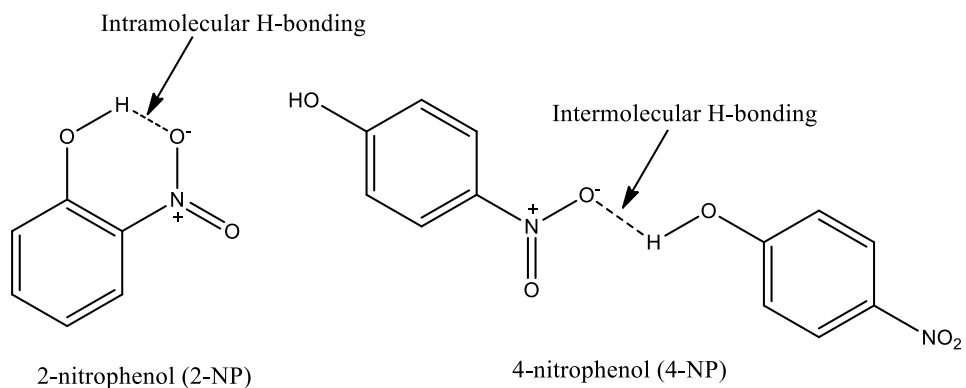


Fig. S19 Intra and intermolecular H-bonding shown in 2-NP and 4-NP, respectively. The former prevents the availability of phenolic -OH proton more than the latter for interaction with **1**.

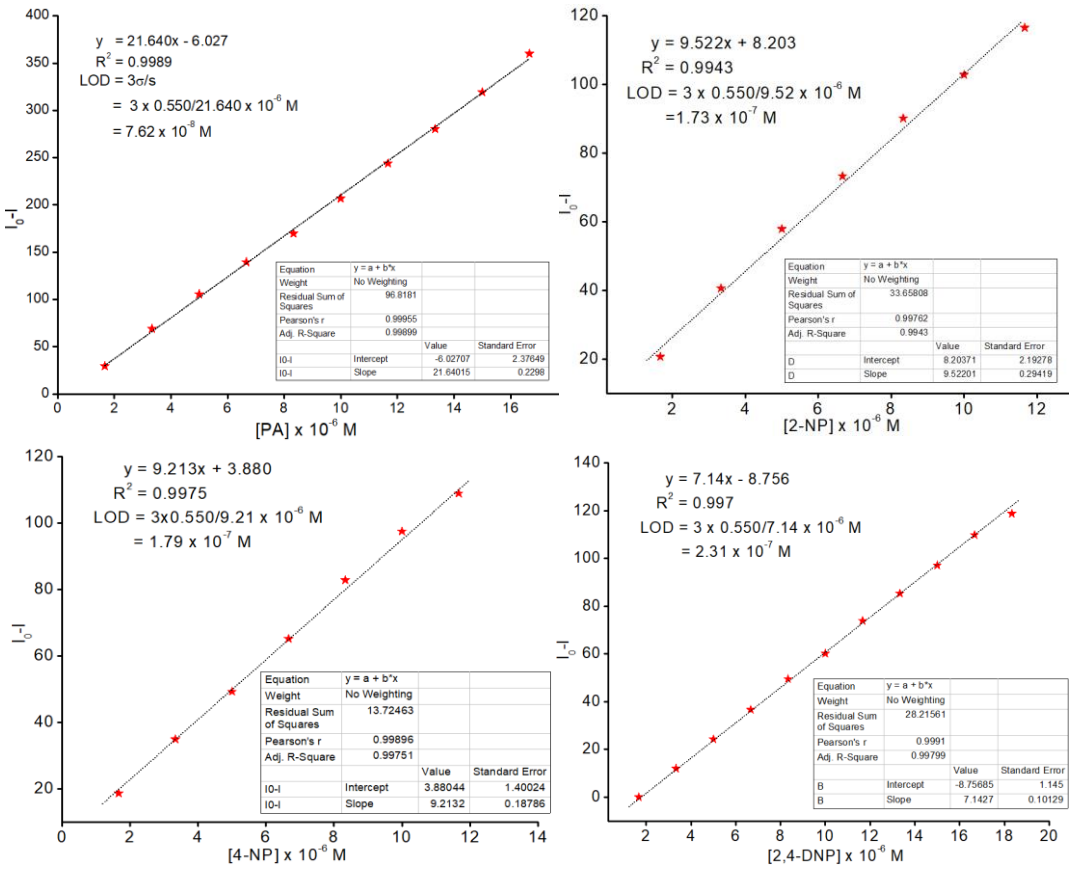


Fig. S20 LOD calculation of **1** for PA; 2-NP; 4-NP and 2,4-DNP. Linear slope obtained between micro molar concentrations from 1.66×10^{-6} to $16.7 \times 10^{-6} M$ of the given analytes were plotted as $I_0 - I$ vs conc.

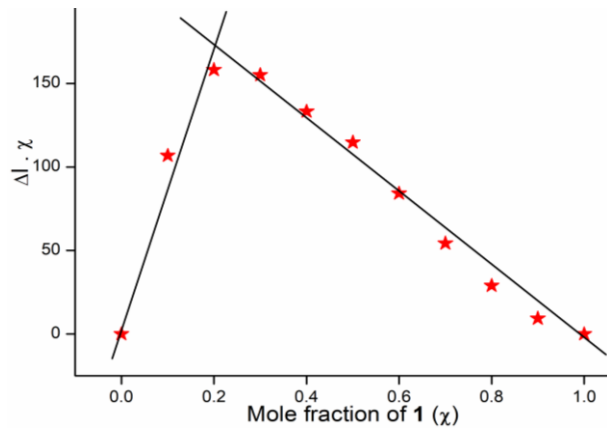


Fig. S21 Job's plot for determining stoichiometries between **1** and PA which signified a ratio of 1:4 for **1**:PA.

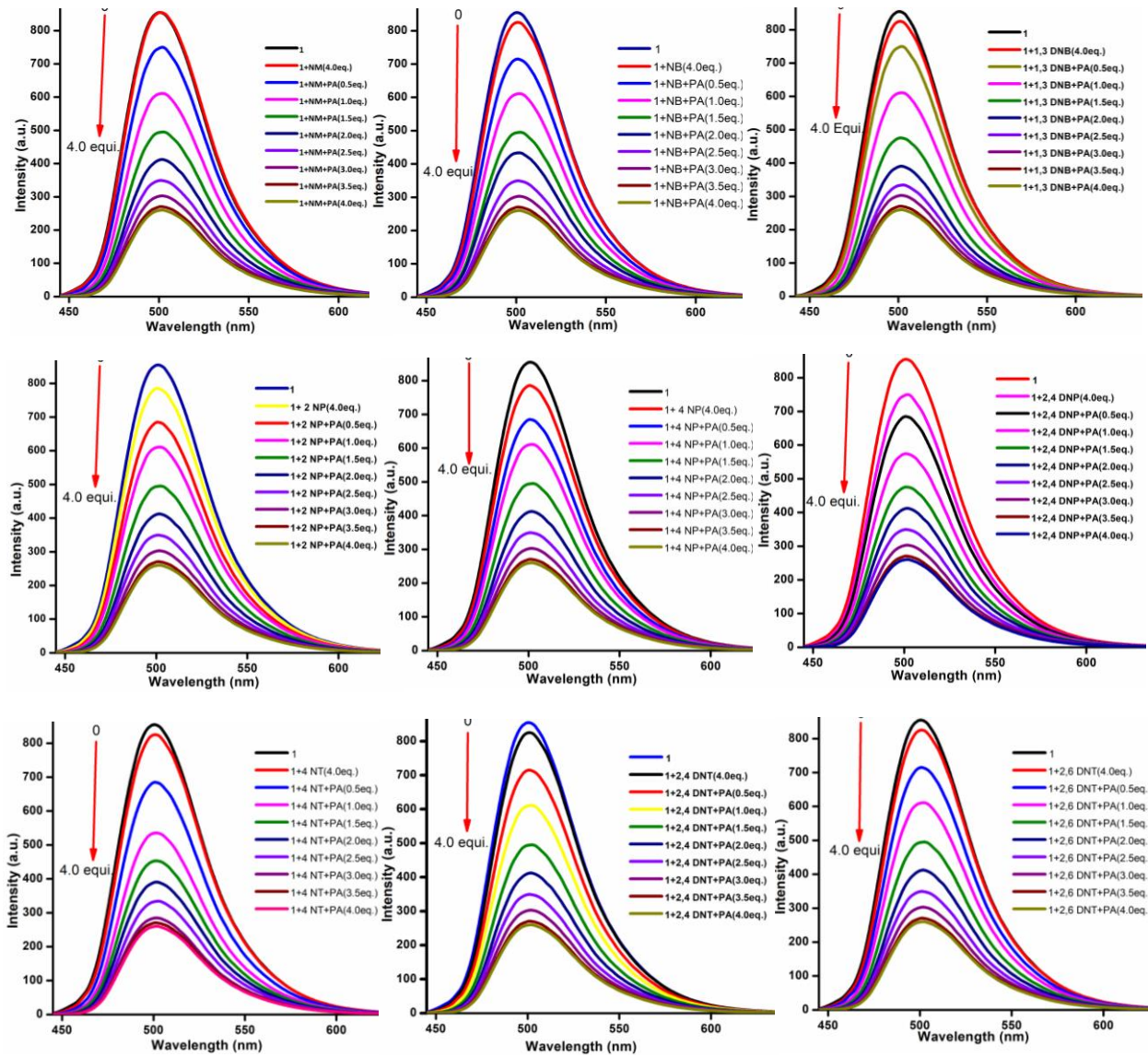


Fig. S22 Fluorescence spectra of **1** ($c, 10^{-5}$ M in EtOH/H₂O) in presence of various NACs (4.0 equiv. of NM, NB, 1,3-DNB, 2-NP, 4-NP, 2,4-DNP, 4-NT, 2,4-DNT) followed by the incremental addition of PA from 0.5 to 4.0 equiv. Fluorescence intensity for **1** was measured on periodic additions of 'PA' in **1** + individual NACs (4.0 equiv.) to show that the respective NACs caused very small quenching and the severe quenching effect (~90-95%) occurred only after subsequent additions of PA (0.5 to 4.0 equiv.). These actually indicated titration of **1** with PA in presence of fixed amount of NACs (4.0 equiv.) to explore the individual interference effect of all NACs.

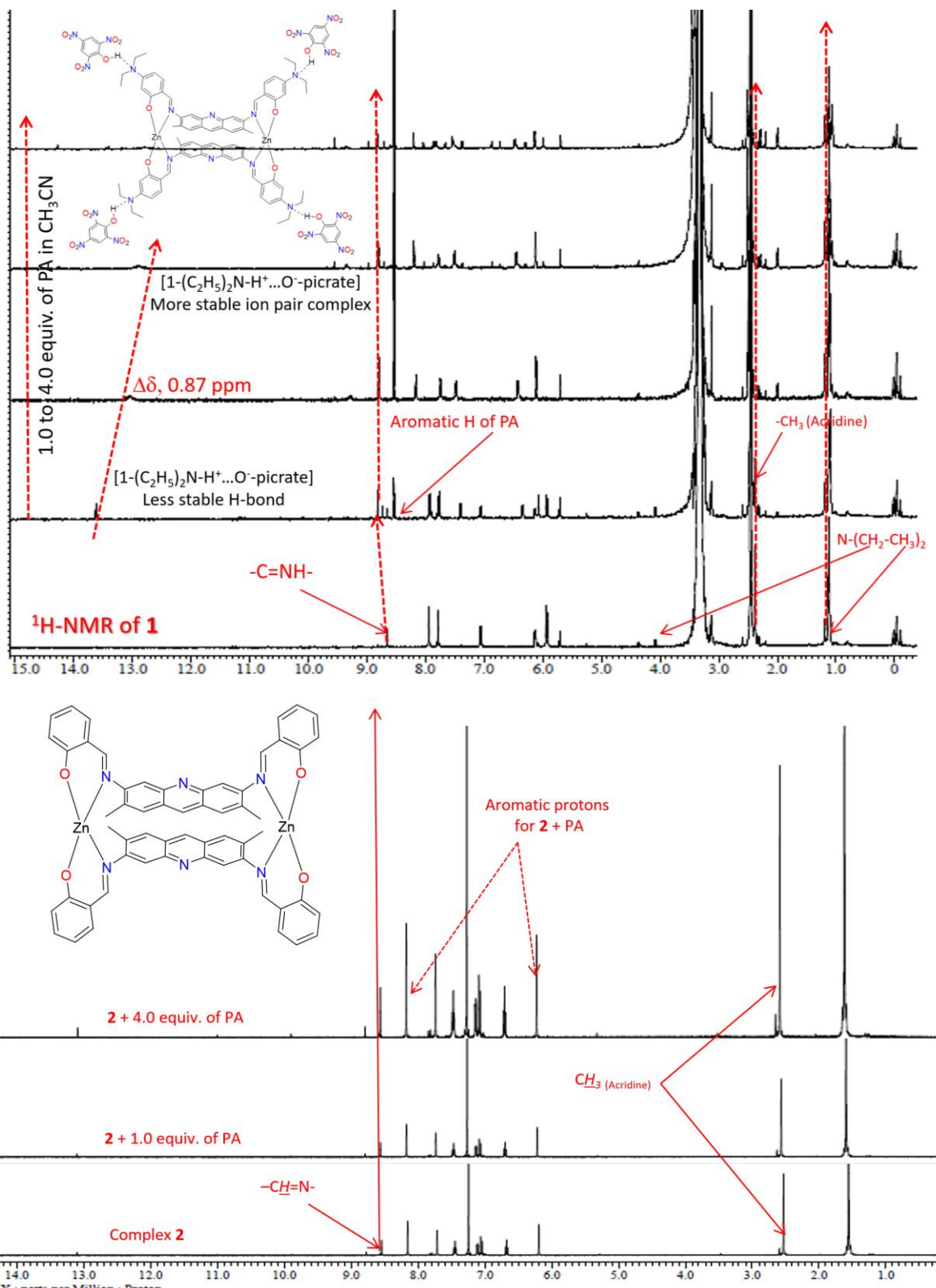


Fig. S23 Overlay diagram of ¹H-NMR titration spectra for **1** (top) and **2** (bottom) with PA (1.0-4.0 equivalent) showing changes in the spectral features of **1** and **2** on PA

addition.

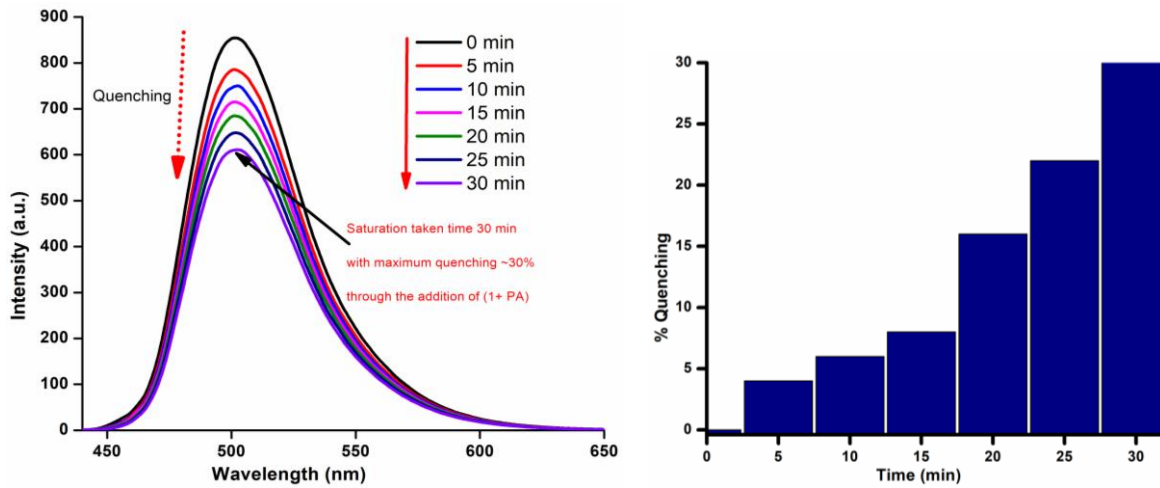


Fig. S24 Fluorescence titration spectra of **1** recorded in vapour phase detection experiment showcasing the maximum fluorescence quenching of ~29-30 % in **1** achieved in 30 min.



Fig. S25 Effect of other NACs on solid surface using Whatman filter paper absorbed with probe **1** (10⁻⁵ M) in EtOH:H₂O (1:1) observed under UV-vis, 365 nm. It signified very strong signaling for PA only and a little with 2,4-DNP. All other NACs displayed negligible change.

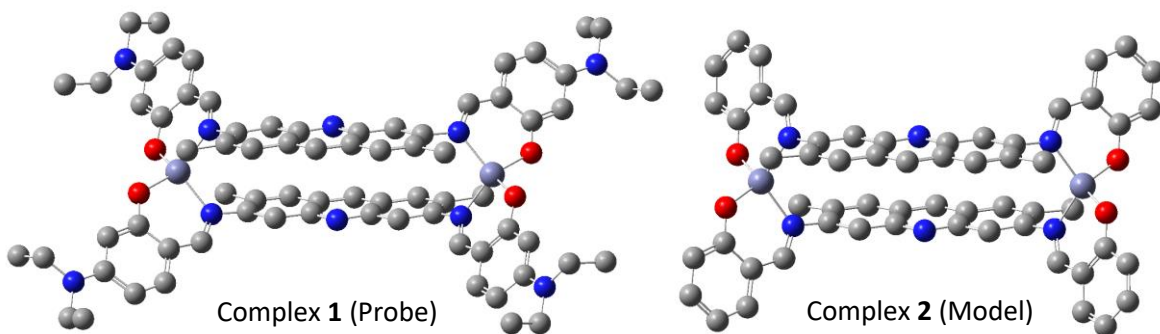


Fig S26 DFT optimized structure of **1** and **2** which showing tetrahedral geometry around the central atom.

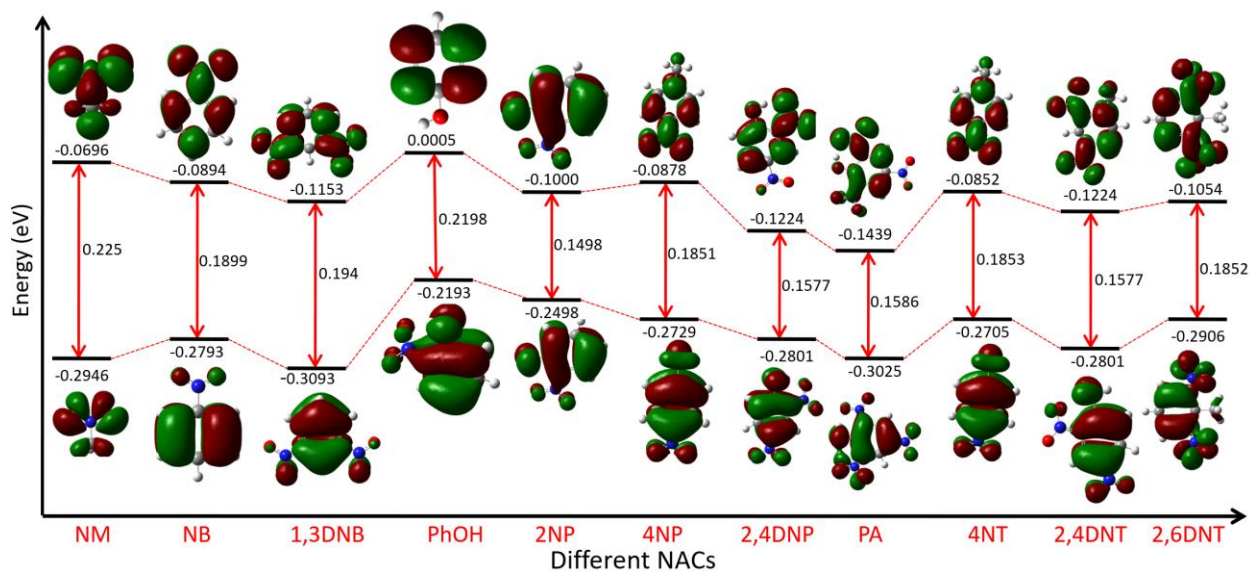


Fig S27 Diagrammatic representation of DFT optimized HOMO-LUMO energies of all NACs which substantiated that PA exhibits lowest energy in comparison to all NACs that enabled it to interact most with HOMO of **1**.

Table T1. Crystallographic data and structural refinement parameters for 1.

Identification code	shelxl
Empirical formula	C ₃₈ H ₄₁ Cl ₂ N ₅ O ₂ Zn
Formula weight	736.1
Temperature	293(2)K
Crystal system	monoclinic
Space group	'P 21/c'
Unit cell dimensions	a = 25.8134(11) Å α = 90° b = 8.4530(5) Å β = 105.653(5)° c = 19.2889(10) Å γ = 90°
Volume	4052.76(59) Å ³
z	4
Density (calculated)	1.21 Mg/m ³
Absorption coefficient	0.774 mm ⁻¹
F(000)	1536
Crystal size	0.20 x 0.10 x 0.05 mm ³
Theta range for data collection	2.4 to 27.1°
Reflections collected	35290
Independent reflections	8301 [R(int) = 0.0734]
Absorption correction	Semi-empirical from equivalents
Max. and min. transmission	0.857 and 0.757
Refinement method	Full-matrix least-squares on F ²
Data / restraints / parameters	8301/0/433
Goodness-of-fit on F ²	0.935
Final R indices [I>2sigma(I)]	R1 = 0.0693, wR2 = 0.1710
R indices (all data)	R1 = 0.1514, wR2 = 0.1959
Largest peak and deepest hole	0.418 and -0.534 e.Å ⁻³
Structure factor coefficient	Fsqd

Table. T2 Selected bond lengths (\AA) for **1**

Atom	Atom	Bond length (A \AA)	Atom	Atom	Bond length (A \AA)	Atom	Atom	Bond length (A \AA)
Zn1	O1	1.905(3)	Cl1	C38	1.643(6)	N5	C31	1.363(5)
Zn1	O2	1.909(3)	C12	C15	1.523(5)	N5	C36	1.433(6)
Zn1	N4	2.014(3)	C28	C33	1.420(5)	N5	C34	1.492(6)
Zn1	N2	2.016(3)	C28	C27	1.422(5)	C9	C8	1.406(6)
O2	C29	1.315(5)	C8	C1	1.392(5)	C9	C10	1.408(5)
O1	C18	1.309(5)	C30	C31	1.382(6)	C25	C26	1.516(6)
N1	C2	1.353(4)	C13	C12	1.368(5)	C29	C30	1.382(5)
N1	C9	1.353(5)	C13	C8	1.424(5)	C29	C28	1.414(5)
N2	C16	1.312(5)	C21	C22	1.344(6)	C34	C35	1.471(7)
N2	C4	1.429(5)	C7	C6	1.409(5)	C17	C16	1.398(6)
N4	C27	1.310(5)	C32	C33	1.342(5)	C2	C3	1.425(5)
N4	C11	1.415(5)	C32	C31	1.421(6)	C4	C3	1.383(5)
N3	C20	1.352(5)	Cl2	C38	1.730(7)	C4	C5	1.409(6)
N3	C25	1.450(5)	C23	C24	1.489(6)	C19	C20	1.409(6)
N3	C23	1.491(6)	C7	C1	1.389(5)	C5	C6	1.359(5)
C11	C10	1.374(5)	C17	C22	1.418(5)	C36	C37	1.513(7)
C11	C12	1.421(6)	C17	C18	1.434(5)	C2	C7	1.415(6)

Table. T3 Selected bond angles (Å) for **1**

Atom	Atom	Atom	Angles [°]	Atom	Atom	Atom	Angles [°]	Atom	Atom	Atom	Atom	Angles [°]
O1	Zn1	O2	102.61(12)	C16	C17	C22	116.6(4)	C31	N5	C36	121.6(4)	
O1	Zn1	N4	130.29(14)	C16	C17	C18	126.8(4)	C31	N5	C34	121.4(4)	
O2	Zn1	N4	97.37(13)	C22	C17	C18	116.5(4)	C36	N5	C34	116.6(4)	
O1	Zn1	N2	97.16(13)	C18	C19	C20	123.8(4)	N1	C9	C8	123.1(4)	
O2	Zn1	N2	130.12(14)	C6	C5	C4	118.9(4)	N1	C9	C10	118.1(4)	
N4	Zn1	N2	103.74(12)	C6	C5	C14	120.2(4)	C8	C9	C10	118.8(4)	
C29	O2	Zn1	125.8(3)	C4	C5	C14	120.9(4)	C11	C10	C9	121.5(4)	
C18	O1	Zn1	126.5(3)	N3	C20	C19	121.9(4)	C11	C38	C12	114.4(4)	
C2	N1	C9	116.8(4)	N3	C20	C21	121.4(4)	C4	C3	C2	120.8(4)	
C16	N2	C4	119.1(3)	C19	C20	C21	116.8(4)	O2	C29	C30	118.6(4)	
C16	N2	Zn1	118.0(3)	C12	C13	C8	121.7(4)	O2	C29	C28	122.6(3)	
C4	N2	Zn1	121.5(3)	C13	C12	C11	119.0(4)	O1	C18	C17	122.0(4)	
C27	N4	C11	117.5(3)	C13	C12	C15	119.3(4)	C19	C18	C17	118.8(4)	
C27	N4	Zn1	118.6(3)	C11	C12	C15	121.7(4)	C7	C1	C8	119.8(4)	
C11	N4	Zn1	121.8(3)	C1	C7	C6	123.2(4)	C22	C21	C20	120.2(4)	
C20	N3	C25	122.1(4)	C1	C7	C2	117.5(4)	N2	C16	C17	129.0(4)	
C20	N3	C23	122.3(4)	C6	C7	C2	119.3(4)	C35	C34	N5	111.8(5)	
C25	N3	C23	115.3(4)	C5	C6	C7	122.4(4)	N5	C36	C37	113.2(5)	
C10	C11	N4	121.9(4)	C29	C28	C33	116.4(4)	C32	C33	C28	123.9(4)	
C10	C11	C12	120.1(4)	C9	C8	C13	118.9(4)	C21	C22	C17	123.8(4)	
N4	C11	C12	118.0(4)	C31	C30	C29	124.2(4)	N4	C27	C28	127.5(4)	
N1	C2	C7	124.1(4)	C33	C32	C31	119.8(4)	C30	C29	C28	118.8(4)	
N1	C2	C3	118.0(4)	C1	C8	C9	118.7(4)	C5	C4	N2	120.0(3)	
C7	C2	C3	117.9(3)	C1	C8	C13	122.4(4)	O1	C18	C19	119.2(4)	
C3	C4	C5	120.7(4)	C29	C28	C27	127.4(4)	C33	C28	C27	116.2(4)	
C3	C4	N2	119.2(4)									

Table T4. Comparison of K_{sv} and LOD for PA detection by **1** with other reported systems.

S. No	Chemo-sensor	Solvent	Analyte	$K_{s-v} (M^{-1})$	Limit of detection (LOD, M)	Ref
1	naphthylvinylpyridine Ligand in Zn(II)/Cd(II)	ACN	Only PA	6.34×10^4	7.2×10^{-7}	5
2	hexaphenyl-benzene derivative	THF/water	Only PA	1.95×10^5	6.87×10^{-9}	6
3	carbazole-N,N-dimethylaniline	DMSO/water	Only PA	1.01×10^7	7.84×10^{-8}	7
4	dimethylamino)-phenyl)diazetyl)-N-(thiophen-2-ylmethyl)benzenesulfonamide	CH ₃ CN	Only PA	1.35×10^4	1.48×10^{-5}	8
5	tetraphenylethylene (TPE)	water	PA against TNT and DNT	5.7×10^4	1.45×10^{-9}	9
6	2-hydroxyphenyl benzimidazoles	THF/water	Only PA	-	8.33×10^{-7}	10
7	Cz-4-CF ₃ and Cz-4-CH ₃	water	Only PA	-	5.14×10^{-8}	11
8	tries dimethyl-aminophenyl-benzene	CH ₃ CN/water	PA, TNT, DNT, m-DNB and p-DNB	3.87×10^5	1.5×10^{-6}	12
9	1,8-naphthalimide	DMSO/water	Only PA	2.27×10^7	3.0×10^{-9}	13
10	hydrazono-sulfonamide	THF/water	Only PA	1.0×10^5	0.08×10^{-6}	14
11	2-(4-aminophenyl)-3-(3-(4,5-diphenyl-1H-imidazol-2-yl)-2-hydroxyphenyl) acrylo nitrile (ADHA)	THF/water	Only PA	4.41×10^5	6.26×10^{-9}	15
	2,6-Pyridine-bis-(iminoantipyrine) (PyBAP)		Related to single crystal XRD			16
12	4-(diphenyl-amino)-2-hydroxy benzaldehyde	THF/water	Sensing related to Zn ²⁺ /Cd ²⁺	-	-	17
13	N,N'-di(Octyl)-Perylene-3,4,9,10-Tetracarboxylic bisimide (PDI-4)	DMF	Fluorescence quenching	-		18
14	tetraphenylethylene	water	Only PA	2.7×10^5	0.4×10^{-6}	19
15	Zn ^{II} -metallacycle (complex 1) [(ZnL) ₂] based on acridine yellow G	EtOH/H ₂ O	Only PA	3.44×10^4	7.62×10^{-8}	This work

References;

- (1) Ö. K. Koç, A. Üzer and R. Apak, *ACS Appl. Nano Mater.*, 2022, **5**, 5868–5881.
- (2) D. Nagaraj, R. M. Melavanki, N. R. Patil and R. A. Kusanur, *Spectrochim. Acta A Mol. Biomol. Spectrosc.*, 2014, **130**, 122-128.
- (3) A. S. Tanwar, S. Patidar, S. Ahirwar, S. Dehingia and P. K. Iyer, *Analyst*, 2019, **144**, 669–676.
- (4) S. Yi, H. Li and X. Liu, *RSC Adv.*, 2022, **12**, 10915-10923.
- (5) B. Dutta, A. Hazra, S. Datta, C. Sinha, P. Banerjee, and M. H. Mir, *ACS Appl. Polym. Mater.* 2022, **4**, 2841–2850.
- (6) V. Bhalla, S. Kaur, V. Vij and M. Kumar, *Inorg. Chem.*, 2013, **52**, 4860-4865.
- (7) D. B. C. Leslee and S. Karuppannan, *J. Photochem. Photobiol. A*, 2022, **429**, 113937.
- (8) P. Kumar, D. Arya, D. Nain, A. Singh, A. Ghosh and D. A. Jose, *Dyes Pigm.*, 2019, **166**, 443-450.
- (9) D. Li, J. Liu, R. T. K. Kwok, Z. Liang, B. Z. Tang and J. Yu, *Chem. Commun.*, 2012, **48**, 7167-7169.
- (10) R. Arumugam, P. Nayak, B. Dey, R. Kannan, K. Venkatasubbaiah and V. Chandrasekhar, *Dalton Trans.*, 2023, **52**, 7926-7935.
- (11) P. Gayathri, S. Ravi, P. Nantheeswaran, M. Mariappan, S. Karthikeyan, M. Pannipara, A. G. Al-Sehemi, D. Moon and S. P. Anthony, *Mol. Syst. Des. Eng.*, 2022, **7**, 1277-1286.
- (12) P. Vishnoi, S. Sen, G. N. Patwari and R. Murugavel, *New J. Chem.*, 2015, **39**, 886-892.
- (13) A. Kumar and P. S. Chae, *Sens. Actuators B: Chem.*, 2017, **240**, 1-9.
- (14) S. Dhiman, N. Singla, M. Ahmad, P. Singh and S. Kumar, *Mater. Adv.*, 2021, **2**, 6466-6498.
- (15) S. M. Kumar and S. K. Iyer, *Sens. and Actuators Rep.*, 2023, **6**, 100177.
- (16) J. Pitchaimani, A. Kundu, S. Karthikeyan, S. P. Anthony, D. Moon and V. Madhu, *CrystEngComm*, 2017, **19**, 3557-3561.
- (17) P.S. Hariharan, S. P. Anthony, *Anal. Chim. Acta*, 2014, **848**, 74-79.
- (18) P. S. Hariharan, J. Pitchaimani, V. Madhu and S. P. Anthony, *J. Fluoresc.*, 2016, **26**, 395–401.
- (19) H.T. Feng and Y. S. Zheng, *Chem. Eur. J.*, 2013, **20**, 195-201.